Leaf area index as a function of precipitation within a hydrological model

Tobias Törnros and Lucas Menzel

ABSTRACT

The Leaf Area Index (LAI) was derived from the Normalised Difference Vegetation Index (NDVI) obtained from Advanced Very High Resolution Radiometer (AVHRR) data for the years 1982–2004. The NDVI-derived LAI showed a very good agreement (correlation coefficient r up to 0.96) with MODIS LAI. To address the relation between precipitation and LAI, linear correlation analysis between gridded precipitation and the NDVI-derived LAI was conducted for several land uses and each month of the year. Based on the regression coefficients, LAI could be simulated as a function of precipitation. During validation, the simulated LAI showed a very good agreement ($r \geq 0.75$) with the NDVI-derived LAI. The simulated dynamic LAI was thereafter implemented in a hydrological model. For comparison, a model run with a static LAI without any inter-annual variations was also conducted. During abnormally dry conditions, the dynamic LAI was lower than the static LAI and less transpiration was therefore simulated. It is shown that a dynamic LAI contributes to a more realistic simulation approach during individual weather events but also that in the long run the simulated transpiration is much more strongly influenced by inter-annual variations in weather than by the additional vegetation dynamics in a semi-arid region.

Key words | climate variability, hydrological modelling, Jordan River region, Leaf Area Index (LAI), Normalised Difference Vegetation Index (NDVI)

Tobias Törnros (corresponding author)
Lucas Menzel
Institute of Geography,
Heidelberg University,
Im Neuenheimer Feld 348,
D-69120 Heidelberg,
Germany
E-mail: *tobias.toernros@geog.uni-heidelberg.de*

INTRODUCTION

Leaf area is an essential component with respect to energy, water, and CO_2 exchange between the terrestrial ecosystem and the atmosphere (Bonan 1993). The Leaf Area Index (LAI) is defined as the one-sided leaf area per unit of ground area. The parameter is included in many evapotranspiration models as well as in hydrological and climate models where evapotranspiration is simulated (Kristensen & Jensen 1975; Chase *et al.* 1996; Menzel *et al.* 2009). It is a measure of the vegetation amount and directly influences plant transpiration and interception evaporation.

Several methods are practised to determine LAI with in-situ measurements (Bréda 2003). However, single measurements are often region specific and limited to certain vegetation types. This obstructs the extrapolation and upscaling of the data for use within regional models (Buermann *et al.* 2002). An alternative to in-situ measurements is to derive LAI from the Normalised Difference Vegetation Index (NDVI) obtained from remote sensing (Turner *et al.* 1999; Qi *et al.* 2000; Colombo *et al.* 2003). The index is acquired from the red (R) and near infrared (NIR) reflectance: $NDVI = (NIR - R)/(NIR + R)$, with which LAI is strongly correlated (Jordan 1969). Several NDVI-LAI equations for different biomes have been described (Sellers *et al.* 1996; Myneni *et al.* 1997; Knyazikhin *et al.* 1998). These have been applied to NDVI data obtained from the Advanced Very High Resolution Radiometer (AVHRR) (Buermann *et al.* 2002; Lu & Shuttleworth 2002; Blümel & Reimer 2009), among others.

When implementing the LAI in a hydrological model, the parameter can be either static or dynamic. A static LAI is the same year after year, whereas a dynamic LAI responds to the weather conditions. Although there are many factors that could be considered when determining the weather

doi: 10.2166/nh.2013.143

conditions, precipitation is probably the single most important one in semi-arid regions (Lázaro *et al.* 2001; Anyamba & Tucker 2005; Fabricante *et al.* 2009). Since the relation between precipitation and vegetation varies between plants and during different growth stages (Rosenthal *et al.* 1987), the seasonality has to be taken into account when addressing the correlation between the two parameters (Ji & Peters 2003). Vegetation furthermore responds to precipitation with a time lag, and precipitation should be accumulated over several months (Fabricante *et al.* 2009).

The aim of this study was to implement the LAI as a function of precipitation to use in a hydrological model. The study focused on: (1) deriving LAI from AVHRR NDVI, (2) addressing the relationship between precipitation and the NDVI-derived LAI, (3) simulating LAI as a function of precipitation for time periods where no LAI or NDVI data are available from remote sensing, and (4) including the simulated LAI within a hydrological model. This LAI parameterisation is expected to improve the regional modelling of the water balance in the arid/semi-arid to sub-humid Jordan River region. It is furthermore expected that the hydrological response to climate extremes will be simulated more accurately. This is of importance since several regional climate models predict decreased precipitation by the middle of this century (Krichak *et al.* 2011; Smiatek *et al.* 2011).

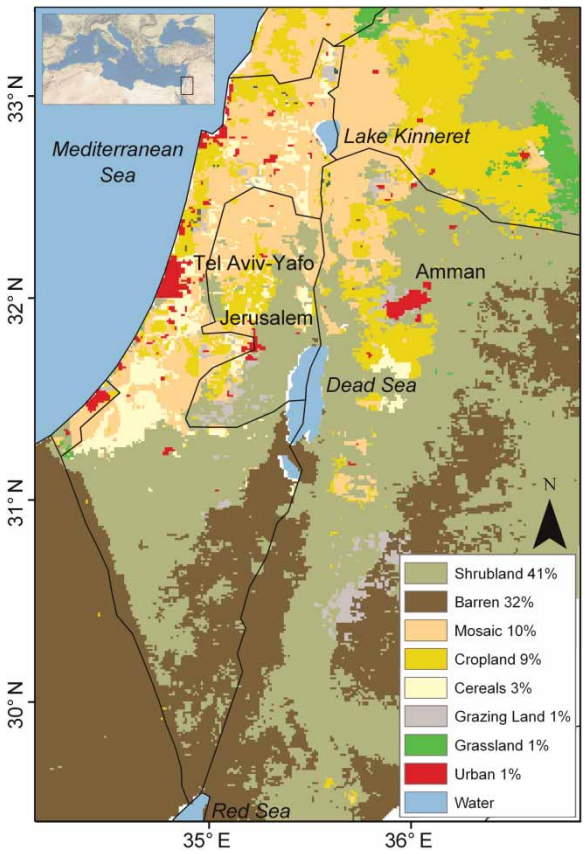

Figure 1 | The location of the study region (based on the Environmental Systems Research Institute (ESRI) World Physical Map) and land uses with spatial coverage in percentages. For visualisation purposes some minor land uses are excluded.

METHODS AND DATA

Study region

The Jordan River region is located in the south-eastern Mediterranean (Figure 1). The region has a Mediterranean climate with hot, dry summers and cool, wet winters where around 90% of the annual precipitation falls between October and March. The latitude (ranging from about 30 to 33 degrees north) and the altitude (ranging from about 400 metres below sea level to 1,800 metres above sea level) further influence the local climate. The annual mean temperature is below 10 °C in the Golan Heights northeast of Lake Kinneret and up to 25 °C in the Jordan Rift Valley stretching between Lake Kinneret and the Red Sea. In the region, two major precipitation gradients exist. They are associated with the orography and winds of different origins (Dahamsheh & Aksoy 2007). The annual precipitation is above 700 mm in the Golan Heights and below 50 mm at the Red Sea. The precipitation also decreases eastwards. The study area can be divided into three climate regions referring to sub-humid (annual precipitation above 450 mm), semi-arid (250–450 mm), and arid (<250 mm) conditions (Figure 2). The arid region is almost exclusively covered by the vegetation-scarce land-use types: shrubland and barren. Only small patches of grazing land and (irrigated) farmland are present. In the sub-humid and semi-arid regions, the farmlands are widespread. In this study, the farmlands are categorised as cropland (covering 9% of the total study area), cereals (3%), and mosaic (10%), which is a mixture of cropland, forests, shrubland, and grassland. The main vegetation period follows the wet season in winter and spring, but the farmlands are commonly cropped more than once a year. During the wet season, rain-fed

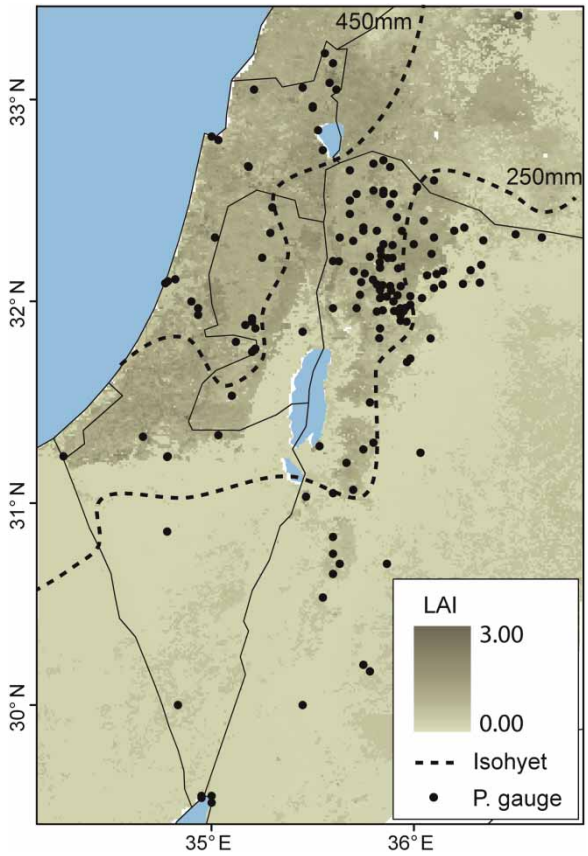

Figure 2 | Simulated annual maximum LAI for the year 2004 and isohyets referring to sub-humid (annual precipitation above 450 mm), semi-arid (250–450 mm), and arid (<250 mm) conditions. The figure also shows the spatial distribution of the precipitation gauges.

winter wheat is grown to a large extent. In the dry summers, other crops dominate and irrigation is required. Since no data on irrigation were available in this study, no attempts have been made to separate the influences of precipitation and irrigation on vegetation growth. Hence, it was assumed that inter-annual variation in vegetation is due to precipitation and not irrigation.

One of the first steps within this study was to prepare a dataset on precipitation. In order to do this, an interpolation method described in Menzel *et al.* (2009) and Wimmer *et al.* (2009) was applied.

Precipitation interpolation

To address the spatio-temporal relation between rainfall and LAI, a gridded data set on precipitation was required. In this study, precipitation data from over 130 gauges were available with daily resolution (Figure 2). Since the region has two distinct precipitation gradients and the gauges are unevenly distributed and frequently contain data gaps, an interpolation method that aims at identifying an appropriate interpolation technique for each single day was applied (Menzel *et al.* 2009; Wimmer *et al.* 2009). By considering the factors elevation and distance to coast as well as the longitude and latitude of the precipitation gauges, the data of each single day were tested for a spatial trend ($p < 0.05$ in the F-test). If the data had a spatial trend, Universal Kriging was applied. If the data had no spatial trend but a variogram could be fitted to the data, Ordinary Kriging was chosen instead. If a variogram could not be fitted to the data, the third to fifth choices of interpolation technique were ordinary least squares, inverse distance weighting, and global mean, respectively. By choosing the most appropriate interpolation technique for each single day, daily precipitation grids ($1\,\text{km} \times 1\,\text{km}$) were prepared for the years 1961–2001. The daily grids were thereafter aggregated (summed) to monthly values to coincide with the temporal resolution of the LAI data.

Deriving LAI from AVHRR NDVI

LAI data are available from the Moderate Resolution Imaging Spectroradiometer (MODIS) sensor from 2002; data on NDVI go further back in time. To get full use of the available data, LAI was therefore derived from AVHRR NDVI. The Global Inventory Modeling and Mapping Studies (GIMMS) NDVI (Pinzon *et al.* 2005; Tucker *et al.* 2005) is a global product based on AVHRR images. It is available from 1981 and has a temporal resolution of two images per month and a spatial resolution of 8 km. LAI was derived from GIMMS NDVI according to a method described in Stöckli & Vidale (2004) and Los (1998). LAI can be defined as:

$$\text{LAI} = \text{LAIg} + \text{LAIs} + \text{LAId} \quad (1)$$

where LAIg is the LAI of the green portion of the canopy, LAIs is the stem area index, and LAId is the dead LAI. Both LAIs (Table 1) and the parameterisation of LAId were adopted from Stöckli & Vidale (2004). During vegetation growth, LAId has a value of 0.0001. During

Table 1 | Land use specific parameters. $NDVI_{min}$ and $NDVI_{max}$ were derived from the AVHRR sensor and $LAIg_{max}$ from the MODIS sensor. LAIs was adopted from Stöckli & Vidale (2004)

Parameter	Grazing land	Mosaic	Shrubland	Barren	Cereals	Cropland
$NDVI_{min}$	0.09	0.21	0.09	0.07	0.10	0.10
$NDVI_{max}$	0.62	0.69	0.38	0.14	0.63	0.62
$LAIg_{max}$	3.50	2.80	2.30	0.50	2.70	2.30
LAIs	0.05	0.05	0.05	0.05	0.05	0.05

vegetation decay, LAId is set to half of the decrease in LAIg between the previous and current time steps. LAIg can be derived from the Fraction of Photosynthetically Active Radiation (FPAR) absorbed by green leaves by applying a logarithmic relationship (Myneni & Williams 1994; Sellers *et al*. 1996; Stöckli & Vidale 2004):

$$\mathrm{LAIg} = \frac{\log\left(1 - \frac{\mathrm{FPAR}}{vcf}\right)\mathrm{LAIg}_{\max}}{\log(1 - \mathrm{FPAR}_{\max})} vcf \quad (2)$$

where $FPAR_{max}$ is a land-use independent constant set to 0.95, $LAIg_{max}$ is a land-use specific maximum LAIg value, and *vcf* is the vegetation-cover fraction of each pixel. FPAR was derived from AVHRR NDVI according to Sellers *et al*. (1996):

$$\mathrm{FPAR} = \frac{\mathrm{NDVI} - \mathrm{NDVI}_{\min}}{\mathrm{NDVI}_{\max} - \mathrm{NDVI}_{\min}}(\mathrm{FPAR}_{\max} - \mathrm{FPAR}_{\min}) + \mathrm{FPAR}_{\min} \quad (3)$$

where $FPAR_{min}$ is a land-use independent constant set to 0.01. $NDVI_{min}$ and $NDVI_{max}$ are land-use specific constants derived from AVHRR NDVI (Table 1). For consistency, all NDVI values lower than $NDVI_{min}$ were set to $NDVI_{min}$ and all NDVI values greater than $NDVI_{max}$ were set to $NDVI_{max}$.

The *vcf* informs about the greenness of the pixel, that is, how much of the pixel is vegetated. The *vcf* was derived for each single year between 1982 and 2004 according to Stöckli & Vidale (2004):

$$vcf = \max(\mathrm{FPAR})/\mathrm{FPAR}_{\max} \quad (4)$$

where max(FPAR) is the annual maximum FPAR value of a pixel (ranging from 0.01 to 0.95 according to Equation (3)). $FPAR_{max}$ is a constant value set to 0.95, as before.

The parameter $LAIg_{max}$ was derived from MODIS LAI based on an assumption. Since LAId and LAIs are much smaller than LAIg for periods with high vegetation, it was assumed that $LAI = LAIg = LAIg_{max}$ for a fully vegetated pixel during the vegetation peak. When deriving $LAIg_{max}$, it was also necessary to consider that the AVHRR sensor has a coarser spatial resolution (8 km) than the MODIS sensor (1 km). A coarser resolution implies a higher degree of mixed pixels and introduced biases (Chen *et al*. 2002) due to bare soil, among other things. In other words, the maximum LAI is expected to be lower for the AVHRR sensor than for the MODIS sensor. Initially, $LAIg_{max}$ was set to the 98 percentile MODIS LAI obtained separately for each land use (Sellers *et al*. 1996). When comparing the NDVI-derived LAI with 1 year of MODIS LAI, these values were thereafter adjusted for certain land uses.

Linear regression analysis between precipitation and LAI

To address the correlation between precipitation and LAI, both the precipitation grids and the NDVI-derived LAI grids were aggregated (mean value) according to land use. For 15 years of data (1982–1996, hereafter referred to as the calibration period), monthly regression analyses were thereafter conducted between accumulated precipitation p_{acc} and NDVI-derived LAI according to:

$$\mathrm{LAI} = \beta_0 + \beta_1 p_{\mathrm{acc}} + \varepsilon \quad (5)$$

where LAI is a land-use average NDVI-derived LAI, ε is prediction error, and β_0 and β_1 are regression coefficients corresponding to the intercept and the slope of the regression line, respectively. The parameter p_{acc} was

defined as precipitation accumulated over 5 months according to:

$$p_{\mathrm{acc}i} = \sum_{i=1}^{180} p_{i-1} + p_{i-2} + p_{i-3} + p_{i-4} + p_{i-5} \quad (6)$$

where p is the land-use average precipitation of month i and 180 is obtained by 15 years of monthly data ($15 \times 12 = 180$). Excluding the precipitation of the present month allowed a short time lag between precipitation and LAI development to be taken into account. Since the relationship between precipitation and LAI varies with the plant's growth stage, the correlation analyses were conducted separately for each month of the year. As a null hypothesis, no correlation between p_{acc} and the NDVI-derived LAI was assumed. The p-value was derived to test this hypothesis. Although not further addressed in this paper, it was elaborated on different time-lags and accumulation periods. In the end, Equation (6) was shown to result in the highest correlation between precipitation and the NDVI-derived LAI.

Simulating LAI as a function of precipitation

With known β_0 and β_1 coefficients, LAI could be simulated as a function of accumulated precipitation according to:

$$\mathrm{LAI}_{\mathrm{dyn}} = \beta_0 + \beta_1 p_{\mathrm{acc}} \quad (7)$$

where $\mathrm{LAI}_{\mathrm{dyn}}$ is a simulated dynamic LAI responding to precipitation and both β_0 and β_1 are specific for each land use and month of the year. LAI was simulated for the time period 1982–2001 and for all land uses. To address the importance of the inter-annual variation in monthly LAI, the dynamic LAI was compared with a static LAI ($\mathrm{LAI}_{\mathrm{sta}}$) parameterisation, that is, an average $\mathrm{LAI}_{\mathrm{dyn}}$ year without any year-to-year variations. Both $\mathrm{LAI}_{\mathrm{dyn}}$ and $\mathrm{LAI}_{\mathrm{sta}}$ were compared to the NDVI-derived LAI by deriving the correlation coefficient for the calibration (1982–1996) and validation (1997–2001) periods.

Observe that $\mathrm{LAI}_{\mathrm{dyn}}$ is a land-use specific mean value for each month. When preparing a spatially distributed LAI product to use within the hydrological model, the spatial variability within each land-use class was assumed to be related to the *vcf* value of each grid cell. The *vcf* grids derived from AVHRR data had a spatial resolution of 8 km, therefore a new and static $1\,\mathrm{km} \times 1\,\mathrm{km}$ *vcf* map was prepared from MODIS data on FPAR for the year 2004 (Equation (4)). This year was chosen since it was relatively wet and the influence of irrigation was therefore assumed to be lower. For each time step, $\mathrm{LAI}_{\mathrm{dyn}}$ was spatially distributed by dividing it by the land-use average *vcf*. The quotient was thereafter multiplied by the *vcf* of each grid-cell.

Hydrological model

TRAIN is a physically based hydrological model that has been applied among others to address the hydrological impact of land-use change in the Jordan River region (Menzel *et al.* 2009). The model requires daily data on precipitation, temperature, relative humidity, wind speed, and global radiation as input. Information regarding soil depth, water-holding capacity of the soil, and LAI is also essential. Model outputs are plant transpiration including interception evaporation, bare soil evaporation, percolation, and runoff. Although the model is able to simulate the demand for irrigation water, this study focused on the relation between precipitation and LAI as well as transpiration under natural conditions. Hence, irrigation was neither simulated nor addressed. The model was set up for the Jordan River region on a 1 km spatial scale and the years 1961–1990. Since the model runs on a daily basis, the monthly simulated LAI was linearly interpolated to daily values. In order to address the potential benefits of having a dynamic LAI with inter-annual variations, the model was run twice: first with $\mathrm{LAI}_{\mathrm{dyn}}$ and thereafter with $\mathrm{LAI}_{\mathrm{sta}}$.

RESULTS

Comparing LAI from two different remote sensors

When deriving LAI from AVHRR NDVI, several parameters had to be obtained. Values of $\mathrm{NDVI}_{\mathrm{min}}$ and $\mathrm{NDV}_{\mathrm{max}}$ were obtained from the $8\,\mathrm{km} \times 8\,\mathrm{km}$ AVHRR NDVI. It can be seen that all land uses have low $\mathrm{NDVI}_{\mathrm{min}}$ values as a result of the dry summers with low vegetation (Table 1). The lowest values are obtained for the land-use

classes barren (0.07) and shrubland (0.09), which together dominate the arid parts of the study region. The land-use classes which are mainly located in the semi-arid and sub-humid regions have higher values. The highest $NDVI_{min}$ value is obtained for the land-use class mosaic (0.21), which is a mixture of cropland, forests, shrubland, and grassland. The relatively high value may be explained by irrigated double cropping and the fact that the forest retains its needles during the dry summer. As expected, barren land and shrubland also have the lowest $NDVI_{max}$ values (0.14 and 0.38, respectively) whereas the highest values are obtained for mosaic (0.69) and cropland (0.62).

Once the required parameters had been obtained, LAI could be derived from AVHRR NDVI (Figure 2). A comparison between the NDVI-derived LAI and MODIS LAI was done visually and by determining the correlation coefficient for the year 2004. At first, NDVI-derived LAI tended to be higher than MODIS LAI due to an overestimation of $LAIg_{max}$ as a result of different spatial resolutions of the original data sets (see methods and data). To obtain a better fit between the series, $LAIg_{max}$ was therefore adjusted (lowered) for certain land uses. The final $LAIg_{max}$ values range from 0.50 for barren to 3.50 for grazing land (Table 1). A visual comparison of the series shows that there is in general a very good correspondence between the AVHRR and MODIS data with regard to vegetation phenology, including the minimum and maximum LAI values (Figure 3). Some differences can also be noticed, however: the NDVI-derived LAI tends to reach its annual maximum earlier than the MODIS LAI; it also tends to be lower than the MODIS LAI during summer. Despite these disparities, the correlation coefficient r ranges between 0.86 and 0.96 and indicates a good to very good correlation between the series. Only for the land-use class barren is there no correlation ($r = -0.09$).

Linear regression analyses between precipitation and LAI

Fifteen years of data (1982–1996) were used to derive linear regressions between monthly accumulated precipitation and monthly NDVI-derived LAI. The obtained intercept β_0 (Table 2) and slope β_1 (Table 3) coefficients, as well as the correlation and p-value (Table 2), differ between land uses and the month of the year. This demonstrates the importance of conducting monthly correlation analysis and that a simple linear correlation assuming the same intercept and slope for every month of the year could not be fitted to the data. It can also be seen that the relation between precipitation and LAI is strongest during the wet season. In November and April, the correlation is statistically significant for a majority of the land uses (Table 2). In the dry and vegetation-scarce autumn between August and October, no significant relation is obtained for any of the land uses. As expected, the intercept coefficient β_0 is higher for relatively vegetation-rich land uses than for the scarcely vegetated land uses – shrubland and barren. The values are highest during the vegetation peak (March–April) and lowest at the beginning of the wet

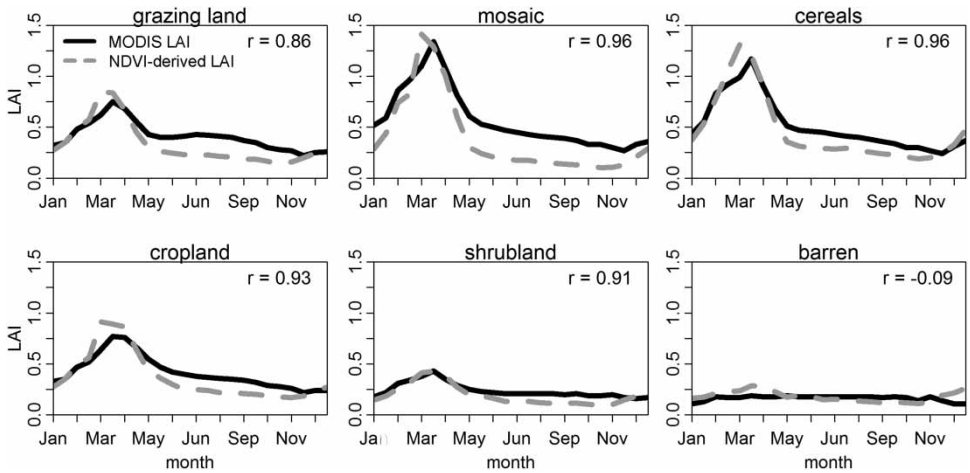

Figure 3 | MODIS LAI and AVHRR NDVI-derived LAI for the year 2004; r is the correlation coefficient between the series.

Table 2 | The interception coefficient β_0 derived for each month and the six major land uses

Month	Grazing land	Mosaic	Shrubland	Barren	Cereals	Cropland
Jan.	0.25*	0.26	0.17	0.19	0.39	0.26
Feb.	0.34	0.52	0.17*	0.20	0.72	0.37
Mar.	0.62	1.06	0.26	0.22	1.06	0.66
Apr.	0.38*	0.66*	0.18*	0.17*	0.56*	0.64
May	0.35	0.48	0.24	0.23	0.45	0.46
Jun.	0.27	0.23	0.18	0.19	0.38	0.25*
Jul.	0.30	0.19*	0.14	0.15	0.41	0.26*
Aug.	0.34	0.20	0.15	0.16	0.39	0.26
Sep.	0.26	0.17	0.14	0.14	0.32	0.24
Oct.	0.21	0.13	0.13	0.14	0.24	0.20
Nov.	0.17*	0.10*	0.12*	0.14	0.21*	0.17*
Dec.	0.19*	0.12*	0.14	0.17	0.25*	0.20

The asterisk (*) indicates a significant correlation (p-value < 0.05) between accumulated precipitation and NDVI-derived LAI.

Table 3 | The slope coefficient β_1 derived for each month and the six major land uses

Month	Grazing land	Mosaic	Shrub-land	Barren	Cereals	Cropland
Jan.	6.12	5.83	5.14	−0.55	6.60	2.94
Feb.	7.96	4.95	10.17*	1.86	4.56	3.42
Mar.	2.30	0.04	6.46	0.25	1.63	1.04
Apr.	10.54	7.79	11.39	3.90	10.00	4.53
May	4.33	2.17	3.37	−0.70	3.21	5.00
Jun.	3.63	3.04	2.26	−0.77	1.63	6.11
Jul.	2.54	4.92	2.94	2.29	2.11	4.27
Aug.	−1.42	4.55	0.49	1.50	4.04	3.21
Sep.	−7.20	−1.07	1.34	4.45	−7.27	−1.65
Oct.	−14.51	−3.65	−3.58	−5.50	−13.63	0.89
Nov.	20.48	19.76	18.55	11.91	16.34	21.74
Dec.	10.13	11.06	7.90	2.80	9.43	6.07

The values have been scaled with a factor of 10^4.

season (November) before vegetation starts to develop (Table 2). The same tendency can be observed in the slope coefficient β_1 (Table 3). During the main vegetation period, the coefficient is positive, which shows that the precipitation stimulates vegetation growth. In November, β_1 is comparably high, which indicates that vegetation responds quickly to early precipitation. It is also interesting to see that β_1 is negative (although non-significant) between August and October. For certain land uses, this may indicate an intensified irrigation in the absence of precipitation during the previous months.

Simulated LAI

The correlation coefficient between simulated LAI and NDVI-derived LAI was derived for a calibration period (1982–1996) and a validation period (1997–2001). Two LAI parameterisations (LAI_{dyn} and LAI_{sta}) were compared, and the results show that both methods can reproduce the NDVI-derived LAI phenology but only LAI_{dyn} can reproduce the inter-annual LAI monthly variation. As expected, LAI_{dyn} therefore has a stronger correlation with NDVI-derived LAI than LAI_{sta} has. During both calibration and validation, the correlation coefficients between LAI_{dyn} and the NDVI-derived LAI range between 0.75 and 0.94 (Table 4). Although LAI_{sta} does not react to the current weather conditions, the seasonality within the data is strong and the correlation with NDVI-derived LAI is still high, having a correlation coefficient between 0.71 and 0.93 during calibration and between 0.78 and 0.93 during validation. In Figure 4 the LAI_{dyn} is plotted together with the NDVI-derived LAI. The differences in LAI between land uses can be clearly seen: the lowest values are obtained for the vegetation-scarce barren land and shrubland. For these land uses, LAI is below 0.5 and the

Table 4 | The correlation coefficient between simulated (LAI_{dyn} and LAI_{sta}) and NDVI-derived LAI for the calibration (1982–1996) and validation (1997–2001) period and the six major land uses

Method	Period	Grazing land	Mosaic	Shrubland	Barren	Cereals	Cropland	Average
LAI_{dyn}	Cal.	0.91	0.94	0.89	0.75	0.93	0.92	0.89
	Val.	0.91	0.94	0.92	0.75	0.93	0.91	0.89
LAI_{sta}	Cal.	0.89	0.93	0.84	0.71	0.91	0.90	0.86
	Val.	0.89	0.93	0.87	0.78	0.91	0.89	0.88

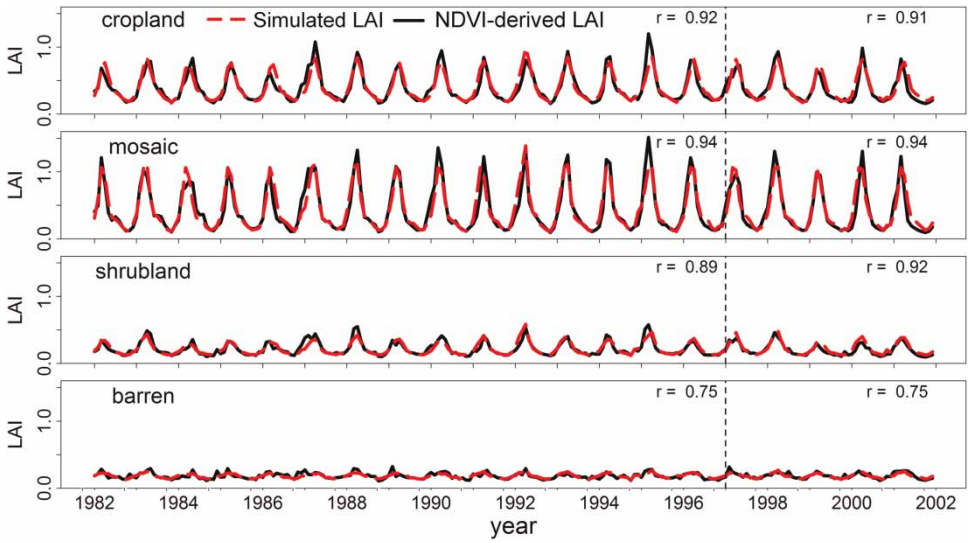

Figure 4 | Simulated LAI (LAI_{dyn}) and NDVI-derived LAI for selected land uses. The time period 1982–1996 was used for correlation analyses and the years 1997–2001 for validation.

variation between years is, especially for barren land, low. For the vegetation-richer land uses, the dynamic is also higher. For cropland, LAI ranges between 0.2 and 1.2, and a clear inter-annual variation can be observed. Mosaic is the land use having the highest LAI values and the largest difference between summer and winter (around 0.2 and 1.5, respectively). A general observation for all land uses indicates that the inter-annual variation is reproduced fairly well by LAI_{dyn} but the vegetation peak for cropland and mosaic is occasionally underestimated. This might be an effect of irrigation; hence it cannot be explained by precipitation and the method applied to simulate LAI. Figure 5 demonstrates that there is an evident relation also between LAI_{sta} and NDVI-derived LAI. Furthermore, it is indicated that LAI_{dyn} is more realistic since LAI_{sta} cannot address the inter-annual variations of the monthly NDVI-derived LAI.

Simulated LAI in a hydrological model

In order to address the importance of an appropriate LAI parameterisation, a model sensitivity analysis was performed with regard to LAI. Several model runs were conducted for an average wet year. Between each run, LAI was varied between ± 5, 10, 15, 20, and 25% while observing the relative changes in the output parameters. The result shows a clear response in the aggregated values of transpiration and interception evaporation

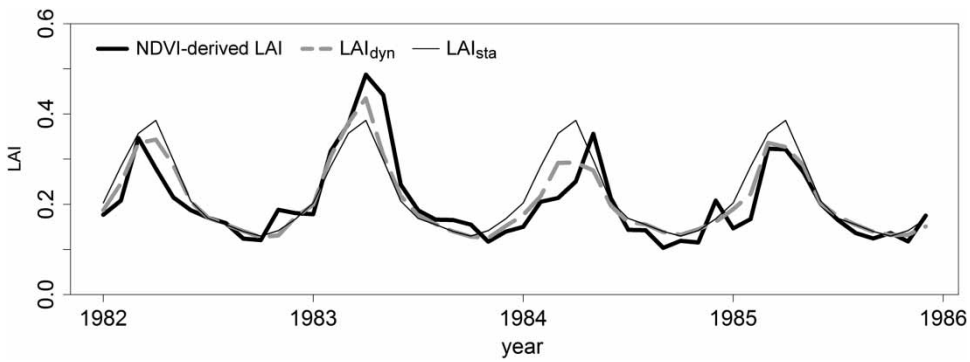

Figure 5 | Four years of NDVI-derived LAI and simulated LAI for the land-use type shrubland. A dynamic LAI was simulated as a function of precipitation (LAI_{dyn}). For comparison an average and static LAI (LAI_{sta}) without any year-to-year variations was used.

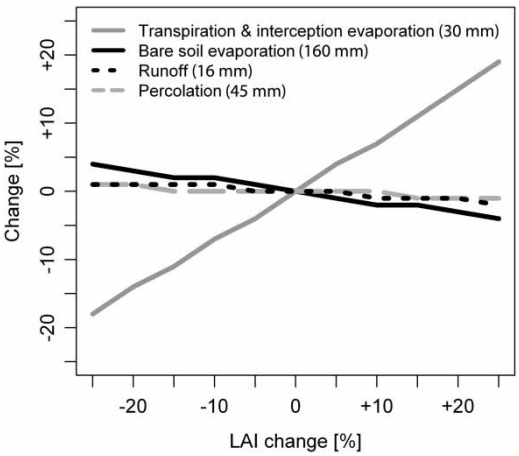

Figure 6 | Sensitivity analysis of the hydrological model TRAIN. The model was run for an average wet hydrological year, for which the simulated fluxes are given in mm. LAI was varied between ± 5, 10, 15, 20, and 25% to address the model's sensitivity to changes in vegetation.

(Figure 6). Transpiration increases quickly with increases in LAI; although this is not surprising it shows that the LAI is a sensitive model parameter and that an appropriate parameterisation is essential when simulating transpiration. As more water is allocated to transpiration; bare soil evaporation, runoff, and percolation all decrease as LAI is increased. The response is relatively slow, however, which means that these parameters are less sensitive to changes in LAI.

To address the difference between two LAI parameterisations, the hydrological model TRAIN was run twice: once with LAI_{dyn} and once with LAI_{sta}. When the evaluation was done according to long-term average conditions, it could be seen that the difference between the model runs is small since less vegetation in one year is compensated for by more vegetation in another year (not shown). Instead, the focus has to be on shorter time periods (e.g. years) addressing certain weather events. Figure 7 shows the annual natural transpiration simulated for one abnormally dry (1983/1984) and one abnormally wet (1968/1969) hydrological year based on the model run with LAI_{dyn}. In the arid south-eastern region, the vegetation is scarce and a high share of precipitation evaporates from bare soil (not shown). Hence, the annual transpiration is lower than 50 mm for both the abnormally dry and the abnormally wet year. In the semi-arid region, more water is available. Thus, both LAI and transpiration are higher and a clear

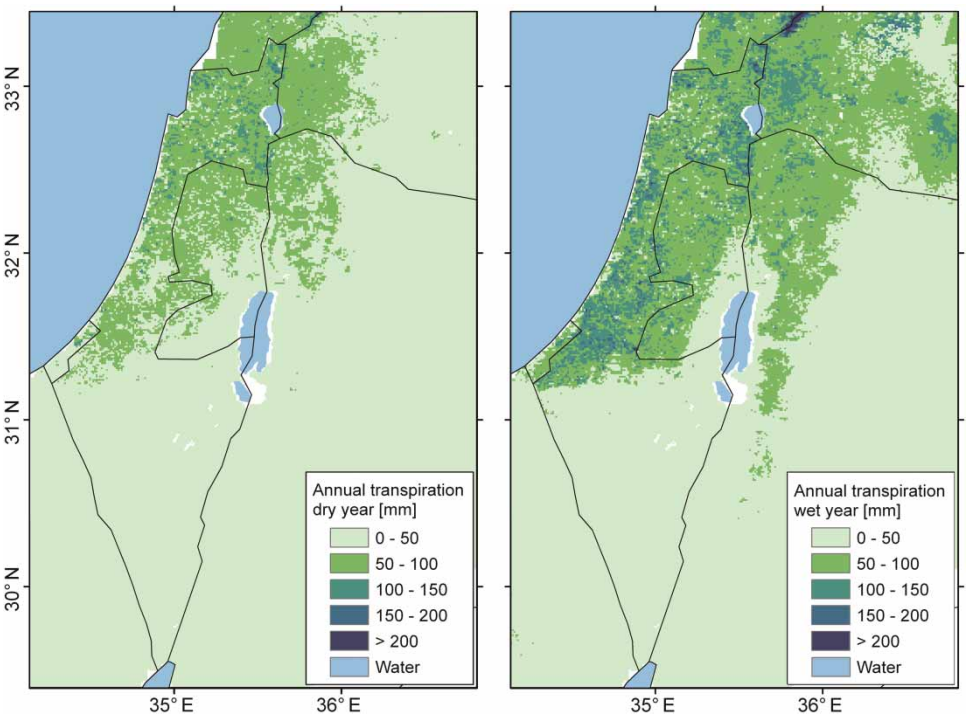

Figure 7 | Annual natural transpiration (without irrigation) simulated for one abnormally dry (left) and one abnormally wet hydrological year (right).

difference can be seen between the years. During the abnormally dry year, the annual transpiration is up to 100 mm. This value is only exceeded for a few scattered pixels. During the wet year the transpiration is higher, being mostly between 100 and 150 mm. The area with an annual transpiration above 50 mm is further extended to the east and to the south in the Jordan Highlands. Around Lake Kinneret and between the Mediterranean and the Dead Sea the annual natural transpiration rate exceeds 150 mm.

Simulated transpiration was also aggregated according to land use, with the land-use types naturally having different LAI and being influenced by different precipitation patterns because of their spatial extent. To address the difference between the model runs, the ratios LAI_{dyn} to LAI_{sta} and LAI_{dyn}-transpiration to LAI_{sta}-transpiration were plotted for the abnormally dry (1983/1984) and the abnormally wet (1968/1969) hydrological year (Figure 8). In general, the transpiration anomalies follow the changes in LAI, which once again demonstrates the parameters' sensitivity and the importance of an appropriate LAI parameterisation. During the abnormally dry conditions, LAI_{dyn} is, as expected, lower than LAI_{sta} (negative anomaly). The clearest difference can be observed in winter and spring, when both LAI_{dyn} and LAI_{dyn}-transpiration occasionally are up to 20% lower than LAI_{sta} and LAI_{sta}-transpiration, respectively. The land use barren, however, is permanently under water stress and no clear difference in transpiration can be observed between the model runs. September is an exception; however, the precipitation amount during this month is close to zero. During abnormally wet conditions, LAI_{dyn} is instead higher than LAI_{sta} (positive anomaly). For both cropland and mosaic, LAI_{dyn} and LAI_{dyn}-transpiration are up to 20% higher than LAI_{sta} and LAI_{sta}-transpiration, respectively. The corresponding value for shrubland is around 10–15%. Generally, this plot alone cannot show whether the lower transpiration rate during the abnormally dry year is due to lack of rainfall or an effect of the lower LAI. However, during the wet year and at the end of the growing season, a sudden drop in transpiration is simulated (for all land uses except barren land) mainly due to a shortage of water, not due to decreases in LAI. This is an effect of the relatively high LAI and transpiration rate earlier in the season. With higher LAI, simulated transpiration occurs at a higher rate, which depletes the soil moisture water storage, that is, the water available for transpiration.

The two model runs were further compared. Since the LAI_{sta}-transpiration is a response to weather variability only while the LAI_{dyn}-transpiration relates to vegetation

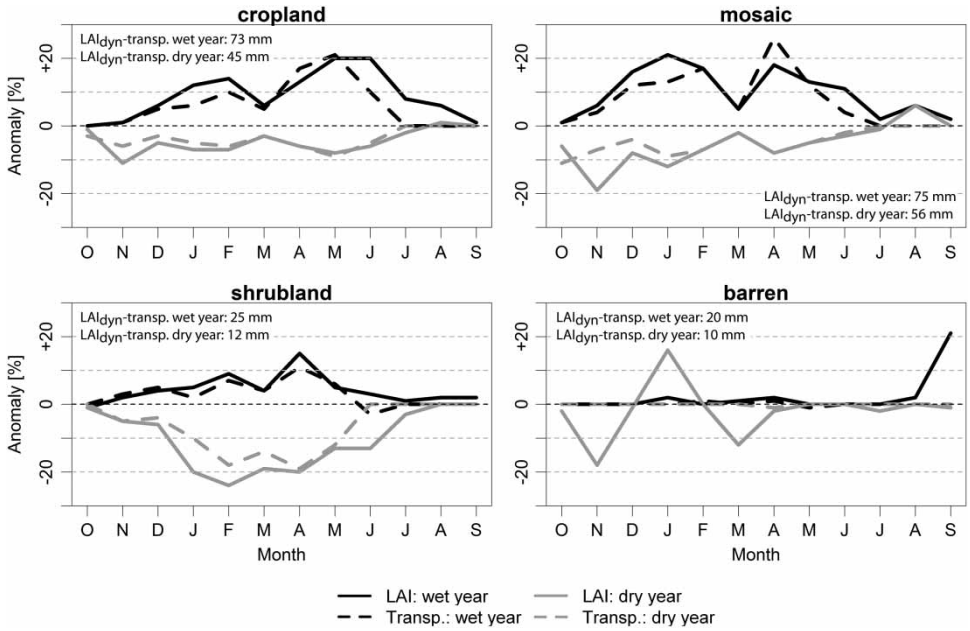

Figure 8 | The two ratios LAI_{dyn} to LAI_{sta} and LAI_{dyn}-transpiration to LAI_{sta}-transpiration for one abnormally dry and one abnormally wet hydrological year.

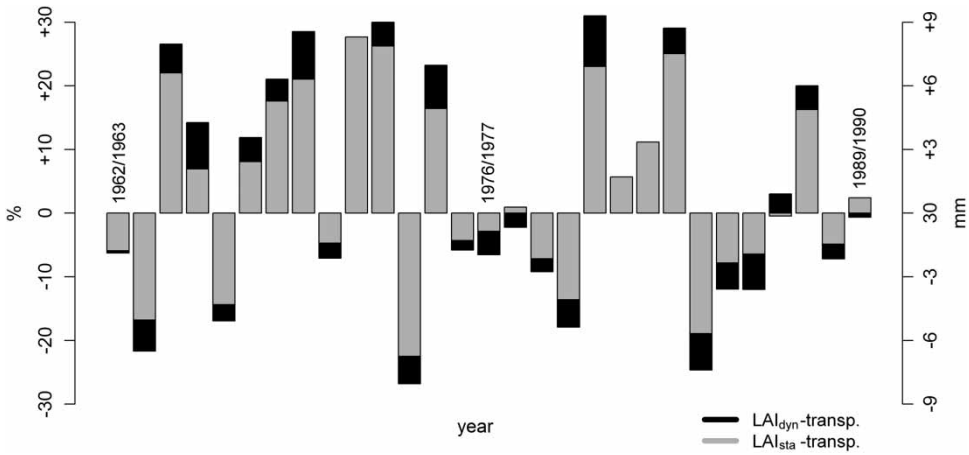

Figure 9 | Annual natural transpiration anomalies expressed as deviation from the long term annual mean. The grey bars (LAI_{sta}-transpiration) are related to weather variability only and the black bars (LAI_{dyn}-transpiration) are additionally related to vegetation dynamics. The figure is based on all land uses and on hydrological years. The anomalies are given both in percentage and mm.

dynamics in addition, a comparison between the two model runs can separate and quantify the influences of weather and vegetation on transpiration. Figure 9 shows the annual natural transpiration anomalies for the whole study region and the years 1961–1990 expressed as deviations from the long term annual mean. It can be seen that the weather-related anomalies are in the range of −22 to 27% and that the additional vegetation-related anomalies range between −6 and 8%. On examining several years including both relatively high and relatively low weather-related anomalies (e.g. the years 1962/1963 to 1965/1966), no clear relation between the amplitude of the weather-related anomaly (LAI_{sta}-transpiration) and the additional vegetation-related anomaly (LAI_{dyn}-transpiration) can be observed and it is clear that a dynamic LAI parameterisation can influence the model results for single years or weather events regardless of the weather condition. Nevertheless, on average the LAI_{sta}-transpiration anomaly is ± 12% and the LAI_{dyn}-transpiration anomaly additionally adds only ± 3%, which shows how (in the long term) the impact of weather variability clearly exceeds the additional impact of vegetation variability when simulating transpiration in the arid to semi-arid/sub-humid region. There are also years when the weather and the vegetation-related transpiration anomalies differ in sign (e.g. 1989/1990). A reason for this could be that not only the annual precipitation but also the precipitation distribution within the year are of importance for the LAI development and the associated transpiration.

DISCUSSION

In the Jordan River region, vegetation has a distinct phenology and the variation between years is much lower than that between seasons. Therefore, the correlation coefficient between LAI_{sta} and NDVI-derived LAI was almost as high as that between LAI_{dyn} and NDVI-derived LAI. However, the results of this study also show how a dynamic LAI addresses the variation in both LAI and transpiration in a more realistic manner. The difference between LAI_{sta}-transpiration and LAI_{dyn}-transpiration was evident when evaluating single weather events like abnormally dry or abnormally wet years, but, in agreement with Guillevic *et al.* (2002), it was also clear that in the long run the impact of weather variability masks the impact of the relatively low variability in vegetation. With a finer spatial resolution, however, the impact of vegetation may be higher. Since the natural vegetation is scarce, it is reasonable to suppose that pixels classified as farmland in reality also have a certain share of non-vegetated areas. Due to these mixed pixels, the remotely sensed LAI and its variability become smoothed and remain lower than measurements with a finer resolution (Sprintsin *et al.* 2007). Hence, coarse resolutions may underestimate the impact of vegetation and transpiration for certain land uses. Differences may also be expected in a humid climate where more water is available for transpiration. It should also be mentioned that not only

precipitation but also irrigation largely contributes to vegetation growth in the region. The applied method assumes that no changes in irrigation practices take place; the method may for example underestimate NDVI if the amount of irrigation is increased. In order to improve the simulation of NDVI for the irrigated land uses, future studies could incorporate irrigation amounts into the accumulated precipitation.

Finally, it is also important to notice that even if the difference between LAI_{dyn}-transpiration and LAI_{sta}-transpiration is considerable when expressed as a percentage, the available water is limited and the regional LAI naturally has low inter-annual variations, and thus the difference between the model runs may be considered low when expressed in actual water amounts.

SUMMARY

NDVI-derived LAI showed high correlations with MODIS LAI when comparing 1 year of data. Based on monthly linear regression analyses between accumulated precipitation and the NDVI-derived LAI, LAI could thereafter be successfully simulated and derived for time periods for which no LAI or NDVI data were available. The simulated LAI was implemented in a hydrological model and comparisons were done with an additional model run having a static LAI without any year-to-year variations. During abnormally dry conditions, the simulated dynamic LAI was lower than the static LAI and therefore lower transpiration was simulated. During abnormally wet conditions, the dynamic LAI and the corresponding transpiration were higher instead. Although it was demonstrated that a simple precipitation–LAI relation improves the hydrological modelling on a regional scale for individual weather events and single years, it was also shown that the impact of weather variability masks the impact of vegetation variability when simulating the long term transpiration under the given semi-arid conditions.

ACKNOWLEDGEMENTS

This study was conducted within the GLOWA Jordan River project funded by the German Ministry of Education and Research (BMBF). The authors are grateful to Stefan Schlaffer for providing spatially interpolated climate data.

REFERENCES

Anyamba, A. & Tucker, C. J. 2005 Analysis of Sahelian vegetation dynamics using NOAA-AVHRRR NDVI data from 1981–2003. *J. Arid Environ.* **63**, 596–614.

Blümel, B. & Reimer, E. 2009 Validation of boundary layer parameters of climate model REMO: estimation of leaf area index from NOAA-AVHRR data for the Baltimos region. *Theor. Appl. Climatol.*, 11.

Bonan, G. B. 1993 Importance of leaf area index and forest type when estimating photosynthesis in boreal forests. *Remote Sense. Environ.* **43**, 303–314.

Bréda, N. 2003 Ground-based measurements of leaf area index: a review of methods, instruments and current controversies. *J. Exp. Bot.* **54**, 2403–2417.

Buermann, W., Wang, Y., Dong, J., Zhou, L., Zeng, X., Dickinson, R. E., Potter, C. S. & Mynenil, R. B. 2002 Analysis of a multiyear global vegetation leaf area index data set. *J. Geophys. Res.* **107**, 16.

Chase, T. N., Pielke, R. A., Nemani, R. & Running, S. W. 1996 Sensitivity of a general circulation model to global changes in leaf area index. *J. Geophys. Res.* **101**, 7393–7408.

Chen, J. M., Pavlic, G., Brown, L., Cihlar, J., Leblanc, S. G., White, H. P., Hall, R. J., Peddle, D. R., King, D. J., Trofymow, J. A., Swift, E., Van der Sanden, J. & Pellikka, P. K. E. 2002 Derivation and validation of Canada-wide coarse-resolution leaf area index maps using high-resolution satellite imagery and ground measurements. *Remote Sense. Environ.* **80** (1), 165–184.

Colombo, R., Bellingeri, D., Fasolini, D. & Marino, C. 2003 Retrieval of leaf area index in different vegetation types using high resolution satellite data. *Remote Sense. Environ.* **86**, 120–131.

Dahamsheh, A. & Aksoy, H. 2007 Structural characteristics of annual precipitation data in Jordan. *Theor. Appl. Climatol.* **88**, 201–212.

Fabricante, I., Oesterheld, M. & Paruelo, J. M. 2009 Annual and seasonal variation of NDVI explained by current and previous precipitation across northern Patagonia. *J. Arid Environ.* **73**, 745–753.

Guillevic, P., Koster, R. D., Suarez, M. J., Bounoua, L., Collatz, G. J., Los, S. O. & Mahanama, S. P. P. 2002 Influence of the interannual variability of vegetation on the surface energy balance: a global sensitivity study. *J. Hydrometeor.* **3**, 617–629.

Ji, L. & Peters, A. J. 2003 Assessing vegetation response to drought in the northern great plains using vegetation and drought indices. *Remote Sense. Environ.* **87**, 85–98.

Jordan, C. F. 1969 Derivation of leaf-area index from quality of light on the forest floor. *Ecology* **50** (4), 663–666.

Knyazikhin, Y., Martonchik, J. V., Myneni, R. B., Diner, D. J. & Running, S. W. 1998 Synergistic algorithm for estimating vegetation canopy leaf area index and fraction of absorbed photosynthetically active radiation from MODIS and MISR data. *J. Geophys. Res.* **103**, 32257–32276.

Krichak, S., Breitgand, J., Samuels, R. & Alpert, P. 2011 A double-resolution transient RCM climate change simulation experiment for near-coastal eastern zone of the Eastern Mediterranean region. *Theor. Appl. Climatol.* **103** (1), 167–195.

Kristensen, K. J. & Jensen, S. E. 1975 A model for estimating actual evapotranspiration from potential evapotranspiration. *Nord. Hydrol.* **6**, 170–188.

Lázaro, R., Rodrigo, F. S., Gutiérrez, L., Domingo, F. & Puigdefábregas, J. 2001 Analysis of a 30-year rainfall record (1967–1997) in semi-arid SE Spain for implications on vegetation. *J. Arid Environ.* **48**, 373–395.

Los, S. 1998 Linkages between global vegetation and climate: An analysis based on NOAA-Advanced Very High Resolution Radiometer data. PhD thesis, Vrije University, Amsterdam, pp. 179.

Lu, L. & Shuttleworth, W. J. 2002 Incorporating NDVI-derived LAI into the climate version of RAMS and its impact on regional climate. *J. Hydrometeor.* **3**, 347–362.

Menzel, L., Koch, J., Onigkeit, J. & Schaldach, R. 2009 Modelling the effects of land-use and land-cover change on water availability in the Jordan River region. *Adv. Geosci.* **21**, 73–80.

Myneni, R. B. & Williams, D. L. 1994 On the relationship between FAPAR and NDVI. *Remote Sense. Environ.* **49**, 200–211.

Myneni, R. B., Ramakrishna, R., Nemani, R. & Running, S. W. 1997 Estimation of global leaf area index and absorbed PAR using radiative transfer models. *IEEE T. Geosci. Remote.* **35**, 1380–1393.

Pinzon, J., Brown, M. E. & Tucker, C. J. 2005 Satellite time series correction of orbital drift artifacts using empirical mode decomposition. In: *Hilbert-Huang Transform: Introduction and Applications* (N. Huang, ed.). World Scientific Publishing, Singapore, pp. 167–186.

Qi, J., Kerr, Y. H., Moran, M. S., Weltz, M., Huete, A. R., Sorooshian, S. & Bryant, R. 2000 Leaf area index estimates using remotely sensed data and BRDF models in a semiarid region. *Remote Sense. Environ.* **73**, 18–30.

Rosenthal, W. D., Arkin, G. F., Shouse, P. J. & Jordan, W. R. 1987 Water deficits effects on transpiration and leaf growth. *Agron. J.* **76** (6), 1019–1026.

Sellers, P. J., Tucker, C. J., Collatz, G. J., Los, S. O., Justice, C. O., Dazlich, D. A. & Randall, D. A. 1996 A revised land surface parameterization (SIB2) for atmospheric GCMs. Part II: The generation of global fields of terrestrial biophysical parameters from satellite data. *J. Climate* **9** (4), 706–737.

Smiatek, G., Kunstmann, H. & Heckl, A. 2011 High-resolution climate change simulations for the Jordan River area. *J. Geophys. Res.* **116**, D16111 (14 pp).

Sprintsin, M., Karnieli, A., Berliner, P., Rotenberg, E., Yakir, D. & Cohen, S. 2007 The effect of spatial resolution on the accuracy of leaf area index estimation for a forest planted in the desert transition zone. *Remote Sense. Environ.* **109**, 416–428.

Stöckli, R. & Vidale, P. L. 2004 European plant phenology and climate as seen in a 20-year AVHRR land-surface parameter dataset. *Int. J. Remote Sens.* **25**, 3303–3330.

Tucker, C. J., Pinzon, J. E., Brown, M. E., Slayback, D., Pak, E. W., Mahoney, R., Vermote, E. & El Saleous, N. 2005 An extended AVHRR 8-km NDVI data set compatible with MODIS and SPOT vegetation NDVI data. *Int. J. Remote Sens.* **26**, 4485–4498.

Turner, D. P., Cohen, W. B., Kennedy, R. E., Fassnacht, K. S. & Briggs, J. M. 1999 Relationships between leaf area index and landsat TM spectral vegetation indices across three temperate zone sites. *Remote Sense. Environ.* **70** (1), 52–68.

Wimmer, F., Schlaffer, S., aus der Beek, T. & Menzel, L. 2009 Distributed modelling of climate change impacts on snow sublimation in northern Mongolia. *Adv. Geosci.* **21**, 117–124.

First received 14 September 2012; accepted in revised form 8 August 2013. Available online 12 September 2013